Myelination of peripheral nerves is controlled by PI4KB through regulation of Schwann cell Golgi function

Takashi Baba[a,1], Alejandro Alvarez-Prats[a,1], Yeun Ju Kim[a], Daniel Abebe[a], Steve Wilson[b], Zane Aldworth[c], Mark A. Stopfer[c], John Heuser[d], and Tamas Balla[a,2]

[a]Section on Molecular Signal Transduction, Eunice Kennedy Shriver National Institute of Child Health and Human Development, National Institutes of Health, Bethesda, MD 20892; [b]In Vivo Science and Delivery, GlaxoSmithKline, Stevenage SG1 2NY, United Kingdom; [c]Section on Sensory Coding and Neural Ensembles, Eunice Kennedy Shriver National Institute of Child Health and Human Development, National Institutes of Health, Bethesda, MD 20892; and [d]Section on Integrative Biophysics, Eunice Kennedy Shriver National Institute of Child Health and Human Development, National Institutes of Health, Bethesda, MD 20892

Edited by Bertil Hille, University of Washington School of Medicine, Seattle, WA, and approved September 18, 2020 (received for review April 17, 2020)

Better understanding myelination of peripheral nerves would benefit patients affected by peripheral neuropathies, including Charcot–Marie–Tooth disease. Little is known about the role the Golgi compartment plays in Schwann cell (SC) functions. Here, we studied the role of Golgi in myelination of peripheral nerves in mice through SC-specific genetic inactivation of phosphatidylinositol 4-kinase beta (PI4KB), a Golgi-associated lipid kinase. Sciatic nerves of such mice showed thinner myelin of large diameter axons and gross aberrations in myelin organization affecting the nodes of Ranvier, the Schmidt–Lanterman incisures, and Cajal bands. Nonmyelinating SCs showed a striking inability to engulf small diameter nerve fibers. SCs of mutant mice showed a distorted Golgi morphology and disappearance of OSBP at the cis-Golgi compartment, together with a complete loss of GOLPH3 from the entire Golgi. Accordingly, the cholesterol and sphingomyelin contents of sciatic nerves were greatly reduced and so was the number of caveolae observed in SCs. Although the conduction velocity of sciatic nerves of mutant mice showed an 80% decrease, the mice displayed only subtle impairment in their motor functions. Our analysis revealed that Golgi functions supported by PI4KB are critically important for proper myelination through control of lipid metabolism, protein glycosylation, and organization of microvilli in the nodes of Ranvier of peripheral nerves.

phosphatidylinositol | Schwann cell | myelination | Golgi | cholesterol

Myelination of peripheral nerves is a complex process requiring a coordinated series of molecular events executed by Schwann cells (SCs). These events start out early in embryonic development and involve the differentiation of SC precursors to mature SCs. During this time, the nerve fibers are arranged according to their diameter by a process called radial sorting, ultimately yielding SCs that are committed either to the myelination program or to the formation of Remak bundles engulfing multiple smaller fibers (1). Improper myelination and axonal sorting defects cause peripheral neuropathies, such as the several forms of Charcot–Marie–Tooth (CMT) disease (2). Since the myelination process requires communication between the axon and the SC, it is not always easy to know whether the pathology is primarily caused by defects in the neurons or in the SCs (3). SC-specific inactivation of some of these genes in mice allowed making distinction between these possibilities (for a list, see table 1 in ref. 1). Such studies helped us better understand the complex biology of the myelination process and identify key molecular steps that could be modified to benefit CMT patients.

Among the genes that are associated with CMT, many control vesicular trafficking (3). Moreover, many signaling events that drive myelination are reminiscent of those found in migrating cells. These include directional protein trafficking, lipid delivery, cell adhesion, and actin cytoskeleton remodeling. Moreover, the advancement of the inner spiral of the tip of the SCs during myelin formation greatly resembles the directional movement of migrating cells driven by phosphoinositide gradients formed between the leading and trailing edges (4). The fine architecture of myelin exemplified by the delicate structure of the nodes of Ranvier requires communication between the axon and the surrounding SCs and relies upon the proper delivery of molecular cues to their final destinations. The Golgi plays an important role in most of these processes. For example, the position of Golgi is determined by the direction of cell migration and also determines the direction of vesicular trafficking and secretion (5, 6). The Golgi is the major site of glycosylation and sorting of cell surface proteins that mediate cell–cell and cell–matrix interactions (7). Moreover, the Golgi is a key organelle for the synthesis and delivery of sphingolipids and an important intermediary station for cholesterol transport from the endoplasmic reticulum (ER) to the plasma membrane (PM) (8).

The minor phospholipid phosphatidylinositol 4-phosphate (PI4P) is a key regulator of Golgi function (9). It plays a role in defining post-Golgi vesicle exit sites and recruits various adaptors for membrane coats (10). PI4P also controls delivery of ceramide, glycosyl ceramide (8, 11) and cholesterol (12) from the ER to the Golgi. Golgi PI4P is made by three distinct PI 4-kinases (PI4Ks): PI4KB, a type III PI4K, and the type II PI4Ks, PI4K2A and PI4K2B (13). PI4K2A and PI4K2B work primarily in endosomes and the trans Golgi network and play important roles in vesicular trafficking pathways, including those important for autophagy (14). PI4KB plays a role in post-Golgi secretion (15) and is an essential host factor for the replication of several

Significance

We identify PI4KB, a phosphoinositide kinase that controls the functions of the Golgi compartment, as a critical regulator of myelination of peripheral nerves. Genetic inactivation of PI4KB, specifically in Schwann cells in mice, causes hypomyelination of large diameter axons and impairs engulfment of small diameter fibers by nonmyelinating Schwann cells. Sciatic nerves of mutant mice show depletion of cholesterol, sphingomyelin and phosphatidylethanolamine, as well as defects in protein glycosylation.

Author contributions: M.A.S. and T. Balla designed research; T. Baba, A.A.-P., D.A., Z.A., and J.H. performed research; Y.J.K., S.W., Z.A., and M.A.S. contributed new reagents/analytic tools; T. Baba, A.A.-P., Z.A., J.H., and T. Balla analyzed data; T. Balla wrote the paper with inputs from T. Baba and A.A.-P.; Y.J.K. contributed to lipidomic analysis; and D.A. assisted with all animal work and experiments.

Competing interest statement: S.W. is an employee of GlaxoSmithKline.

This article is a PNAS Direct Submission.

See online for related content such as Commentaries.

[1]T. Baba and A.A.-P. contributed equally to this work.

[2]To whom correspondence may be addressed. Email: ballat@mail.nih.gov.

This article contains supporting information online at https://www.pnas.org/lookup/suppl/doi:10.1073/pnas.2007432117/-/DCSupplemental.

First published October 26, 2020.

picornaviruses, most likely by helping the virus create the proper lipid composition of its replication organelle (16).

There is little information about the role of the Golgi in peripheral myelination by SCs. The small GTPase Arf1 plays a pivotal role in controlling vesicular trafficking in the Golgi complex (17). SC-specific inactivation of Arf1 or one of its guanine-nucleotide exchange factors, BIG1, in mice has been reported recently, showing delayed initiation of myelination, reduced myelin thickness, and a decreased amount of myelin protein 0 (Mpz) (18). One of the major regulators of Golgi function is the lipid kinase PI4KB (11). To gain further insight in the role of Golgi in peripheral nerve myelination, we created and characterized a mice model with genetic inactivation of PI4KB specifically in SC. These mutant mice develop a myelination defect characterized by thinner myelin of large diameter axons, with gross alterations in the structure of nodes of Ranvier and a striking inability of non-myelinating SCs to wrap small diameter fibers in Remak bundles. These changes were attributed to Golgi functions affecting cholesterol transport, glycosylation, and a hitherto unrecognized role of PI4KB in the SC microvilli at the nodes of Ranvier.

Results

SC-Specific PI4KB Knockout Mice Show Hind Limb Weakness and Decreased Myelin Proteins. We have generated mutant mice with specific deletion of the PI4KB gene in SCs by crossing a mouse line with floxed alleles of the PI4KB gene surrounding exons 6 and 7 (*SI Appendix*, Fig. S1) with a mouse strain that expresses an Mpz promoter-driven Cre recombinase (Mpz-cre) (19). Mice were born at the expected Mendelian ratio and genotyped by PCR to identify the homozygous conditional allele expressing the Cre recombinase ($PI4KB^{f/f}$ mpz-cre^{+}, hereafter referred to as "mutants") (*SI Appendix*, Fig. S1*B*). Mutant mice, but not their heterozygous littermates (for controls both $PI4KB^{wt/wt}$, mpz-cre^{+} or $PI4KB^{wt/f}$, mpz-cre^{+} were used), displayed the clasping reflex (Fig. 1*A*) and showed spasticity in their hind legs with a subtle change in their gate, noticeable already at 3 wk after birth. This phenotype, however, was substantially milder than that observed in our recently described SC-specific PI4KA knockout (KO) mice (20) with no gross difference in the appearance of sciatic nerves (Fig. 1*B*). Nerve conduction velocity measurements on sciatic nerves in situ (20) showed more than 70% decrease in the conduction velocity (Fig. 1 *C* and *D*). Surprisingly, analysis of mice using the rotarod test (at 6 and 11 wk) showed only a small change that became statistically significant only in the group analyzed at 11 wk (Fig. 1*E*).

Western blot analysis of proteins obtained from sciatic nerves of control and mutant mice was performed to assess the effect of PI4KB inactivation in SCs on the major myelin proteins. This analysis performed on 12-wk-old mice showed the decrease in PI4KB (note that the enzyme was only deleted in SCs) (Fig. 1*F*). The amount of PI4K2A, another PI4K that is localized at least partially to the Golgi complex in mammalian cells (10), did not show a compensatory increase; in fact, PI4K2A was also slightly decreased (Fig. 1*F*). There was a massive decrease observed both in the amounts of myelin-basic protein (MBP) and myelin protein 0 (MPZ) compared to controls (Fig. 1*F*). However, the level of PMP22, another important myelin protein component, was increased rather than decreased (see later under *PI4KB KO Suppresses Glycosylation in the Sciatic Nerve*).

Localization of PI4KB to the Golgi and the Node of Ranvier. It was of particular interest to look at the localization of PI4KB in the nerves of wild-type (WT) mice. As shown in Fig. 2*A*, PI4KB was localized to the perinuclear Golgi compartment of SCs (Fig. 2*A*, yellow arrowheads), but, surprisingly, it was even more prominent in the nodes of Ranvier (Fig. 2*A*, green arrowheads) in sciatic nerves of 13-wk-old mice. Such localization of PI4KB was already detected at 3 wk of age. In the nodes of Ranvier, PI4KB showed tight colocalization with the SC microvilli-specific protein, Dystrophin Dp116 (Fig. 2*B*). In nodes of Ranvier, microvilli are emanated from the outer membrane of the SC and are attached to the axolemma marked by voltage-gated ion channels, such as the Na^{+} channel. Double staining with PI4KB and pan-Na^{+} channel antibodies indicated that PI4KB staining was associated with microvilli rather than the axolemma marked by Na^{+} channel staining (Fig. 2*C*). There was no staining of PI4KB in mutant nerves (Fig. 2*C*), also confirming that the PI4KB staining in the nodes of WT mice was indeed associated with SCs and not with the axons. Importantly, the width of the axons at the nodes of Ranvier was significantly expanded (Fig. 2 *C* and *D*), suggesting a microvilli defect.

We also determined the localization of PI4K2A, another PI4K, both in mutant and control sciatic nerves. Fig. 2*E* shows that PI4K2A was localized to the Golgi and also shows punctate staining at the paranode in control cells. Notably, unlike PI4KB, other Golgi markers, such as GM130 (Fig. 2*E*) or giantin (see Fig. 6*D*) were not found in the nodes of Ranvier.

It has been shown that PI4KB interacts with Rab11 and is involved in recruitment of this small GTPase to endosomal compartments (21, 22). Therefore, we determined the localization of Rab11 in the nerves of WT mice and found that it did not localize to the microvilli in nodes of Ranvier but showed prominent staining at the paranodal loops (Fig. 2*E*). This finding did not suggest recruitment of Rab11 by PI4KB to the SC microvilli.

Structural Defects of Mutant Nerves. Phalloidin staining of sciatic nerves from mutant mice showed a greatly aberrant structure with thinner fibers, less pronounced and less spaced Schmidt–Lanterman incisures (SLIs), and largely expanded Cajal bands which were observed in nerves from all ages of animals examined (11 to 40 wk) (Fig. 3 *A* and *C*). It was also notable that sciatic nerves of mutant mice showed many more nuclei. As shown in Fig. 3 *A* and *B*, immunohistochemical analysis revealed significantly smaller footprints of Dystrophin-related protein 2 (Drp2) that is located at the appositions between the outermost layer of myelin and the abaxonal membrane (see schematic in Fig. 3*D*). Accordingly, Western blot analysis of sciatic nerves revealed a substantial decrease in Drp2 compared to controls, consistent with the histological findings (Fig. 3 *E* and *F*).

Electron Microscopy Analysis of Mutant Nerves Revealed Significant Structural Defects. We then conducted electron microscopy (EM) analysis of the sciatic nerve from 8- to 12-wk mutant mice and their control littermates. This analysis showed reduced myelin thickness and increased interstitial space between myelinated fibers (Fig. 4*A*). Calculation of g-ratios (the ratio of the inner axonal diameter to the total outer diameter of the myelin) from the EM images of control and mutant mice showed an increased g-ratio in the mutant nerves that was only apparent with the higher diameter axons (Fig. 4 *B* and *C*). In fact, small diameter axons had often increased myelin thickness (Fig. 4*C*), a difference that was statistically significant. This finding suggested that myelination of mostly the large axons was impaired. Also, closer inspection of the relationship between the axons and myelin revealed several tight appositions between the abaxonal membrane and the outermost myelin membrane in control nerves, but these were rarely observed in the mutants (Fig. 4*D*, green arrows). This was in line with the reduced Drp2-positive areas and expanded Cajal bands observed in the mutant sciatic nerves shown in Fig. 3*A*. Another notable difference between the SCs of mutant vs. WT mice was the great reduction and, in some cases, almost complete lack of caveolae in the mutants (Fig. 4 *D* and *E*, marked with orange).

There was also a change in the organization of the nodes of Ranvier in mutant nerves: The microvilli that SCs send to the

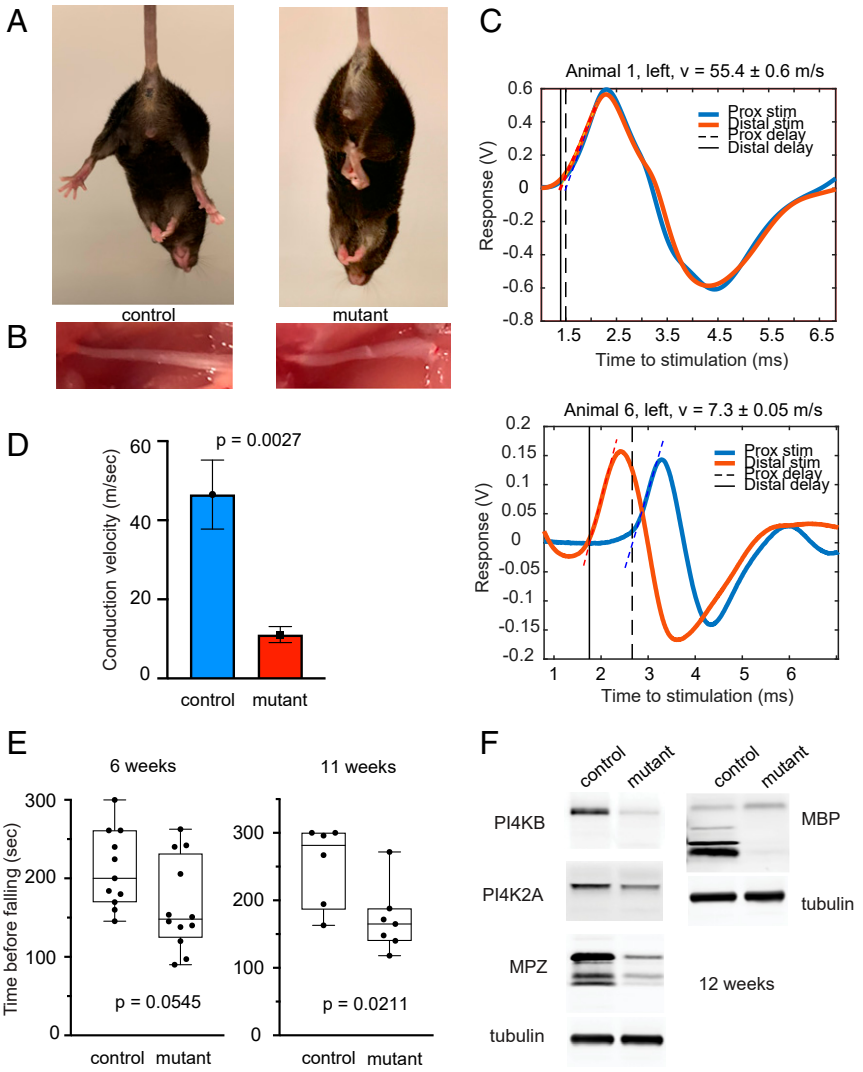

Fig. 1. SC-specific inactivation of PI4KB in mice. (*A*) The 11-wk-old mutant mice show very subtle defects in motor function, but the tail hanging test reveals a functional defect in peripheral nerves. (*B*) There is no major macroscopic difference between control and mutant sciatic nerves. (*C*) Nerve conduction velocity measurements in situ in 11-wk-old mice. Electromyography (EMG) recordings are shown from the same animal after stimulating the sciatic nerve from a proximal (blue) and distal (orange) electrode. The time delay and the distance between the two stimulating points allow calculation of the conduction speed (*Upper*, control; *Lower*, mutant). (*D*) Conduction velocity measurements in 11-wk-old mice (means ± SEM, $n = 6$). (*E*) Rotarod analysis of control and mutant mice at 6 and 11 wk of age. There was a slight difference between the two groups at 6 wk, but it did not reach statistical significance. The difference became statistically significant when tested at 11 wk. (*F*) Western blot analysis shows reduced protein levels of PI4KB and the myelin-specific proteins myelin protein zero (MPZ) and myelin basic protein (MBP) in sciatic nerves of mutant mice. Note that PI4KB was only inactivated in the SCs. There was no compensatory increase in PI4K2A; in fact, its expression was also slightly reduced.

naked part of the axon in control nerves (Fig. 5 *A*–*C*, blue arrows) were either missing or severely underdeveloped, allowing the axons to bulge into the space often showing herniations (Fig. 5 *D* and *E*, orange arrows). In many nodes, the SCs expanded into the node with numerous mitochondria present but did not develop microvilli (Fig. 5*E*, blue arrow). A striking change in the morphology of the Remak bundles was also observed in the mutant mice. While the cytoplasm of nonmyelinating SCs completely surrounded and isolated most of the individual fibers in WT nerves (Fig. 5*F*, cytoplasm is colored blue), the cytoplasm of mutant SCs failed to penetrate between the small nerve fibers and failed to engulf them (shown in Fig. 5*G*, cytosol is colored blue; quantified in Fig. 5*H*) as illustrated in the schematic in Fig. 5*G*. Also prominent was the disintegration of the basal lamina around the Remak bundles.

Loss of PI4KB Leads to Disorganization of the Node of Ranvier. Given the finding of the EM analysis, further studies were performed to analyze the organization of the nodes of Ranvier. For this, we used a pan-Neurofascin antibody along with staining of the Na^+ channels. These studies showed that, while Na^+ channels still lined up in the nodes of Ranvier, they were not as tightly packed and also showed some clustering. Moreover, the axons did not show their normal constriction at these sites but were rather dilated (Fig. 6*A*; also see Fig. 2 *C* and *D*). Pan-Neurofascin staining also showed the lack of axon constriction at the nodes of Ranvier, and the signal was shorter and had a loose organization (Fig. 6 *A* and *B*). The lack of axon constriction could be the consequence of the lack of microvilli and along with a significant decrease in the phalloidin staining at the nodes of Ranvier in the mutant nerves (Fig. 6*C*).

Loss of PI4KB Leads to Disorganization of the Golgi and Mislocalization of PI4P Binding Proteins. Since PI4KB generates PI4P primarily in the Golgi complex and several Golgi proteins require PI4P for their localization or function, we set out to determine the status of the Golgi in the sciatic nerves of control and mutant mice. As shown in Fig. 6*D*, the Golgi marker giantin showed tight perinuclear localization in control nerves whereas its signal and the area stained were both greatly reduced and more dispersed in the mutants. Importantly, the Golgi-localized PI4P-binding protein, GOLPH3 (23), showed a tight Golgi localization but showed no signal in the node of Ranvier in control nerves (Fig. 6*E* yellow arrow). Strikingly, GOLPH3 was undetectable in the nerves of mutant mice (Fig. 6*E*). This prompted us to determine the localization of another PI4P binding Golgi protein, OSBP, which is responsible for cholesterol transport between the ER and the Golgi (24). In control nerves, OSBP

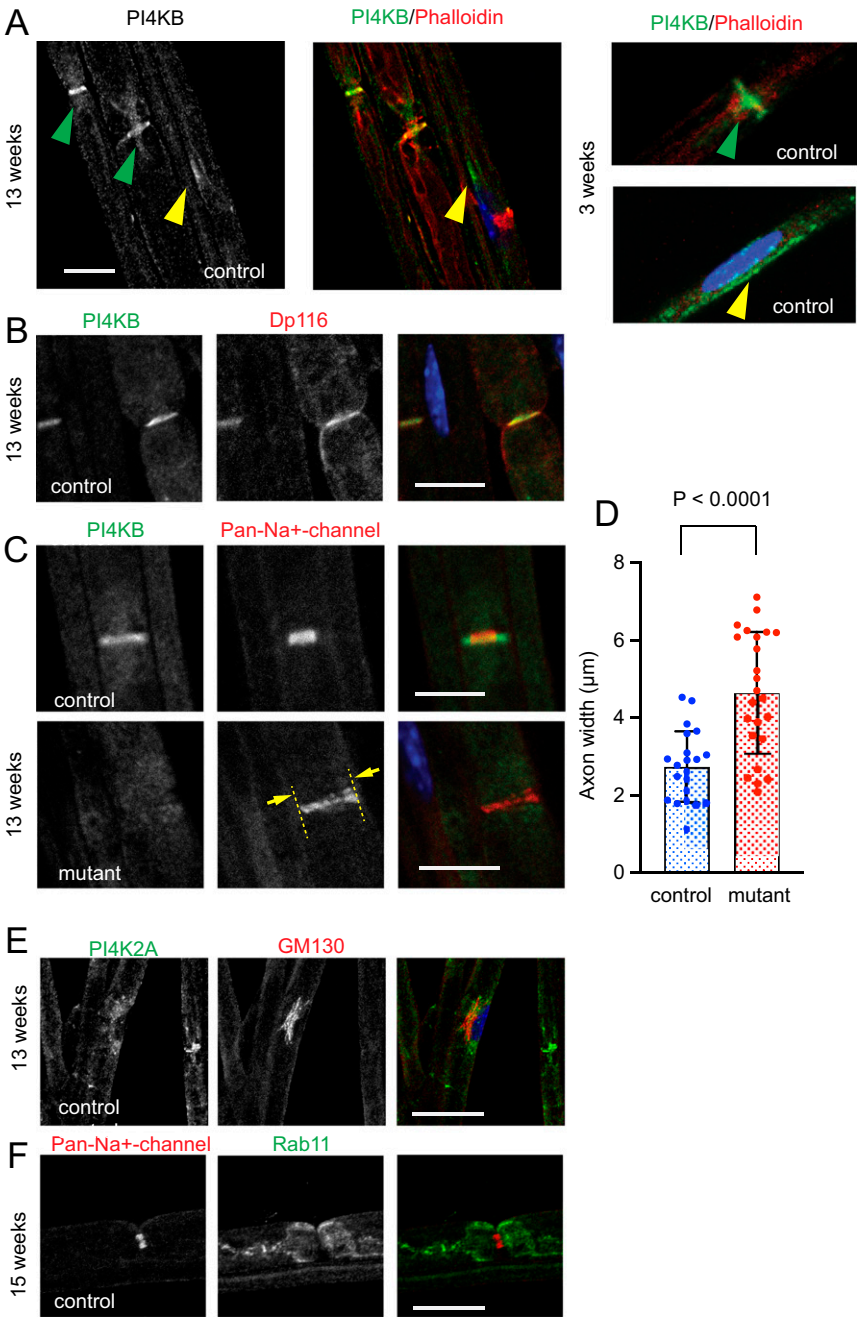

Fig. 2. Localization of PI4KB, PI4K2A, and Rab11 in sciatic nerves of control and mutant mice. (*A*) Teased sciatic nerves from 13-wk-old or 3-wk-old control mice were immunostained with antibodies against PI4KB and with phalloidin. (*Left*) PI4KB distribution in the Golgi (yellow arrowhead) and prominently in the nodes of Ranvier (green arrowheads). (*Center* and *Right*) The overlay (PI4KB, green; phalloidin, red; and nuclei, blue). (*B*) The microvilli-specific protein Dp116 colocalizes with PI4KB at the nodes of Ranvier. (*C*) The pan voltage-gated Na^+ channel is found in the axon, but PI4KB is present in the SC microvilli. Also note the less compact and uneven distribution of the Na^+ channel without the typical narrowing of the axon at the middle of the node in the mutant. The width of the axon is marked by the yellow dotted lines and arrows. (*D*) Statistical analysis on the width of Na^+ channel staining in the nodes of Ranvier (mean ± SD from measurements of 21 and 24 nodes in WT and mutant, respectively, obtained in four different nerve preparations). (*E*) The distribution of PI4K2A is different from that of PI4KB. This enzyme shows a faint signal at the perinuclear Golgi area (marked by the cis-Golgi GM130 staining) and a punctate signal at the paranode in control nerves. (*F*) The distribution of Rab11 (assessed in a 15-wk-old control mice) shows paranodal signal which is different from the localization of PI4KB. (Scale bars: *A*, *E*, and *F*, 20 µm; *B* and *C*, 10 µm.) These images are representatives of what was observed in two separate nerve preparations from different animals immunostained independently.

showed prominent Golgi localization where it tightly colocalized with GM130 (Fig. 6*F*). Similar to GOLPH3, OSBP was not localized to the nodes of Ranvier. However, unlike GOLPH3, the localization of OSBP was not completely eliminated in the mutants, but it was greatly reduced and showed dispersed and punctate staining that no more colocalized with the reduced and shrunk GM130-positive Golgi compartment (Fig. 6*F*).

PI4KB KO Suppresses Glycosylation in the Sciatic Nerve. Given the central role of Golgi in glycosylation and the fact that GOLPH3 has been implicated in the Golgi localization of glycosylation enzymes in yeast (25) and for some of the glycosylation enzymes also in mammalian cells (26, 27), it was important to determine whether glycosylation was affected in mutant nerves. Moreover, complex glycolipids were also shown to play important roles in peripheral nervous system (PNS) myelination (28). Since too many possible candidate proteins can be glycosylated, we took an unbiased approach and analyzed the staining pattern of a series of fluorescein isothiocyanate (FITC)-labeled lectins in teased sciatic nerves of control and mutant animals. Lectins recognize different types of glycosylated proteins and glycolipids on the surface of cells, and several lectins have already been used to explore their specific localizations in peripheral nerves (29), many showing specific enrichment in nodes of Ranvier (30). We used 16 different FITC-labeled lectins to see if any one of them showed a different labeling pattern between control and mutant nerves. Six of these lectins showed a clear labeling pattern in control nerves and were chosen for further analysis (*SI Appendix*, Fig. S2). All of these 6 lectins stained nodes of Ranvier, suggesting enrichment of proteoglycans and/or glycolipids at the

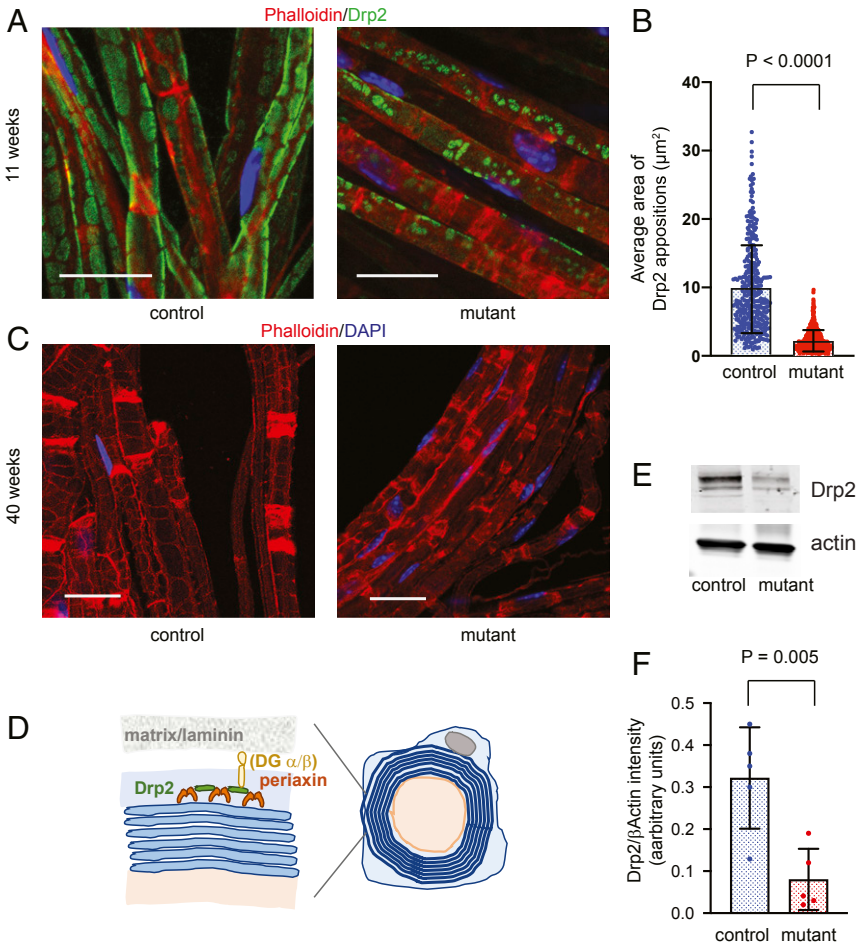

Fig. 3. Structural changes in sciatic nerves in PI4KB mutant mice. (*A*) Teased sciatic nerves from 11-wk-old control and mutant mice were immunostained with an antibody against dystrophin related protein 2 (Drp2) and phalloidin. Note the striking difference in the areas of apposition between the abaxonal membrane and SCs and the consequentially enlarged Cajal bands. Also note the shorter spacing between the Schmidt–Lanterman incisures (SLIs) and the more numerous nuclei. (*B*) Quantification of the Drp2 appositions from two nerve preparations immunostained independently. Mean and SD are shown, $n = 338$ and 479 individual areas from WT and mutant nerves, respectively. (*C*) Similar changes were still observed at a much later stage of 40 wk based on phalloidin staining. (Scale bars: 20 μm in panel *A* and 10 μm in panel *C*.) (*D*) A schematic showing the molecular players forming the appositions: Dystrophin-related protein2 (Drp2); periaxin; and Dystroglycan α and β (DG α/β) (the schematic is drawn after ref. 46). (*E* and *F*) Western blot analysis (*E*) showed a greatly decreased level of Drp2 in the mutant nerves as quantified in *F* (mean ± SD, $n = 5$ animals per group).

nodes. Notably, all of the mutant samples showed higher background staining relative to the control (*SI Appendix*, Fig. S2). This was attributed to the better penetration of the lectin through the thinner myelin and reduced lipid content (see under *Lipid Composition Is Changed in Mutant Sciatic Nerve*). Although slight differences in the staining of all of the tested lectins could be observed between mutant and control nerves, the staining with Lens culinaris agglutinin (LCA) was almost completely eliminated from the nodes of Ranvier in mutant nerves. There was also a substantial difference between the labeling of control and mutant nerves by the peanut agglutinin (PNA) (*SI Appendix*, Fig. S2).

We then used Western blot analysis using selected lectins to see if they showed any change in their binding patterns to proteins isolated from sciatic nerves. Ponceau staining showed some differences in the intensities of some of the higher molecular size bands (between 140 and 240 kDa). Three lectins fused with fluorescein (LCA, PNA, and Jacalin [JAC]) were chosen to use in Western blotting. In the membrane probed with LCA, a prominent difference was observed in the signal of a low molecular mass (~20 to 30 kDa) protein and a change in the region of ~180 kDa (Fig. 7*A*, arrows). We investigated whether the small protein corresponded to PMP22, an important component of the myelin and which is implicated in some forms of CMTs (31). However, as mentioned before, the level of PMP22 was increased rather than decreased in nerves of mutant mice, and its sodium dodecyl sulfate (SDS) migration was not different compared to samples obtained from control mice (Fig. 7*C*). These findings make it unlikely that the small glycosylated protein affected in mutant nerves would be PMP22. Glycosylated proteins of higher molecular mass also showed a difference with the PNA-stained membrane (Fig. 7*B*, top arrows). In addition, there was also a mobility shift in the 120- to 130-kDa region detected both with PNA and JAC (Fig. 7*B*, bottom arrows). Although identification of these proteins will require further work, these results suggested that PI4KB deletion alters the glycosylation pattern of several proteins and could contribute to the morphological changes described above since most cell adhesion molecules undergo glycosylation.

Lipid Composition Is Changed in Mutant Sciatic Nerve. Both cholesterol and ceramide are moved from the ER to the Golgi by nonvesicular lipid transfer using Golgi PI4P as a driving force (8, 12). Reduced Golgi PI4P in PI4KB-deficient SCs could result in improper distribution of cholesterol and ceramide. To investigate this possibility, sciatic nerves from control and mutant mice of 8 and 13 wk were subjected to cholesterol measurements and lipidomic analysis. These data, presented in Table 1, showed an ~60% decrease in the total lipid content of the mutant nerves with a ~70% decrease in cholesterol content, suggesting a relative depletion of cholesterol in the mutant nerves. The more than 50% decrease in the mol% of sphingomyelin (SM) and phosphatidylethanolamine (PE) suggested a specific depletion of these lipids among the other lipid classes.

Discussion

Several genes have been identified that affect myelination of peripheral nerves and cause human neuropathies (2). Some of the diseases, such as CMT type 1, are caused by defects in SC

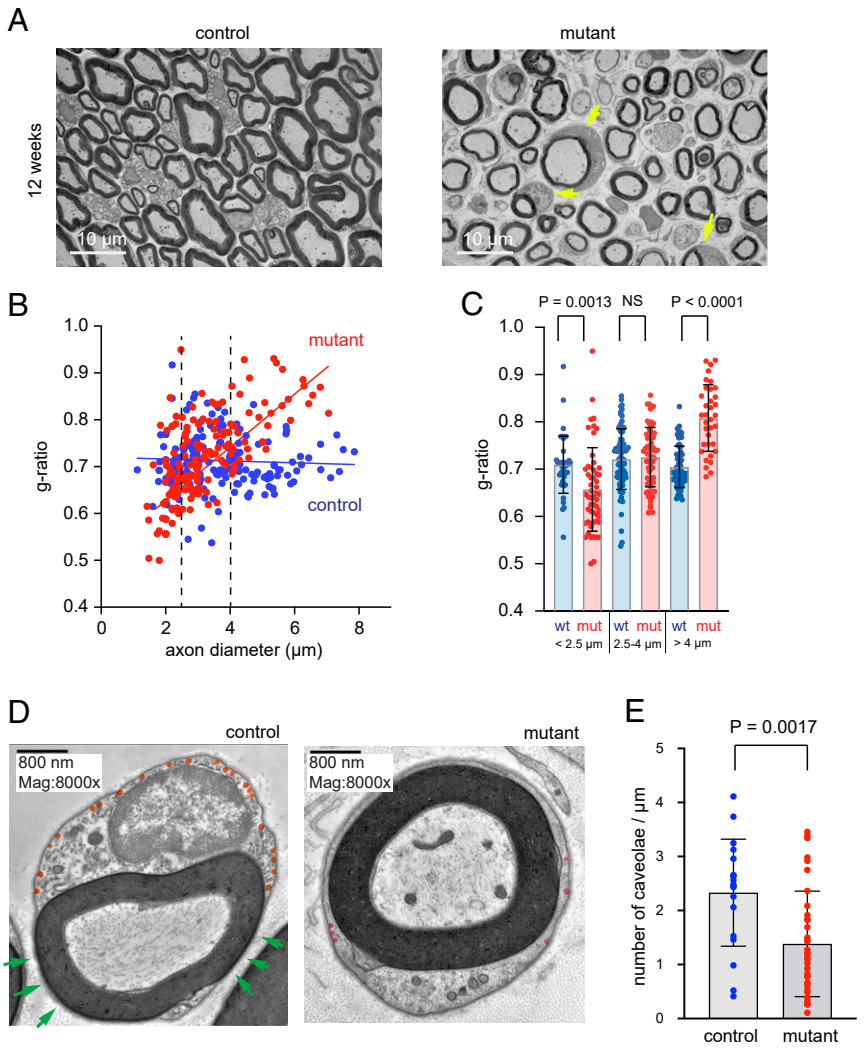

Fig. 4. EM analysis of cross-sections of sciatic nerves from 12-wk-old control and PI4KB mutant mice. (*A*) Cross-sections of sciatic nerves from 12-wk-old control and mutant mice. Note the thinner myelin of the large diameter axons and the massive enlargement of the interstitial space between the axons. Also notable is the enlarged cytoplasm of several SCs in the mutant (yellow arrows). (*B* and *C*) The g-ratios calculated from EM pictures of control (blue) and mutant (red) nerves. Note that larger diameter (>4 µm) axons are hypomyelinated while small diameter (<2.5 µm) axons are more myelinated in the mutants. In panel *B* dotted lines mark these subgroups. NS: not significant. (*D*) Note the lack of appositions between the abaxonal myelin membrane and the SC plasma membrane (green arrows in control) in the mutant nerves. The number of caveolae per micrometer is also greatly reduced in the mutant SCs (marked with orange) as quantified in (*E*) from 19 control and 36 mutant cells (mean ± SD is shown). Images were obtained in two independent nerve preparations from different pairs of mice, and the changes shown are the best representations of at least 10 images obtained in each experiment. (Scale bars are as indicated.)

function while others originate from defects in the neurons themselves (3). Although demyelinating diseases can have several etiologies other than SC functional defects (32), proper SC function is essential for normal myelination and nerve conduction velocity. Genetic targeting of SCs for inactivation of various proteins in mice has been an invaluable tool to better understand the complex process of myelination. Given the unique structure of the myelinating SC and the fact that myelin is formed from the "inside" around the axon, it is rather puzzling how the molecules that are necessary for the myelination process are delivered from their site of synthesis to the most active zone of the SC. It is difficult to study myelination in vitro using cultured SCs, and, therefore, studies on the role of the various trafficking steps in SCs in the whole organism are critical to arrive to a better understanding of both the normal myelination process and the various pathologies found in human myelin-related diseases. Very few studies have focused on the role of Golgi in peripheral nerve myelination (18, 33).

Phosphoinositide lipids (PPIns) are critical in organizing the various trafficking pathways in all eukaryotic cells, including the Golgi (34). The major PPIn in the Golgi is PI4P, a lipid produced primarily by PI4KB and PI4K2A (13). Many studies have focused on the role of PI4KB using cell culture systems, but few have addressed the role of the enzyme in a whole organism. The yeast homolog of PI4KB, called Pik1p, is an essential gene (35) that supports post-Golgi secretion (36). Surprisingly, inactivation of the PI4KB ortholog, called Four-wheel drive (Fwd) in *Drosophila*, is not lethal, but it causes male infertility, due to a block in cytokinesis of spermatocytes (37). It is likely that, in the fly, Fwd shares some functions with the type II PI4K as neither single mutant is lethal (38). There are no studies available on PI4KB function in mammalian organisms.

We have genetically inactivated PI4KB specifically in SCs of mice and characterized the phenotype focusing on the sciatic nerves. These mice display very subtle functional defects that do not show obvious progression with time. Yet the conduction velocity of the sciatic nerves decreased dramatically, and major structural defects are revealed by histochemical and EM analyses. A significant myelination defect was observed in large diameter axons while the myelination of small diameter axons was augmented. The selective impairment of the myelination of larger diameter axons could be an indication that transport of proteins to larger distances is progressively impaired and a compensatory mechanism yields hypermyelination of the smaller diameter axons. There was a prominent loss of contacts between the abaxonal myelin membranes and the SCs, causing an expansion of Cajal bands. Longitudinal sections also revealed expansion of unmyelinated axons at nodes of Ranvier and greatly reduced SC microvilli. One of the most striking differences, however, was observed with the nonmyelinating SCs (Remak bundles) where the SCs were unable to wrap the small diameter fibers, only forming rudimentary extensions reaching between those fibers.

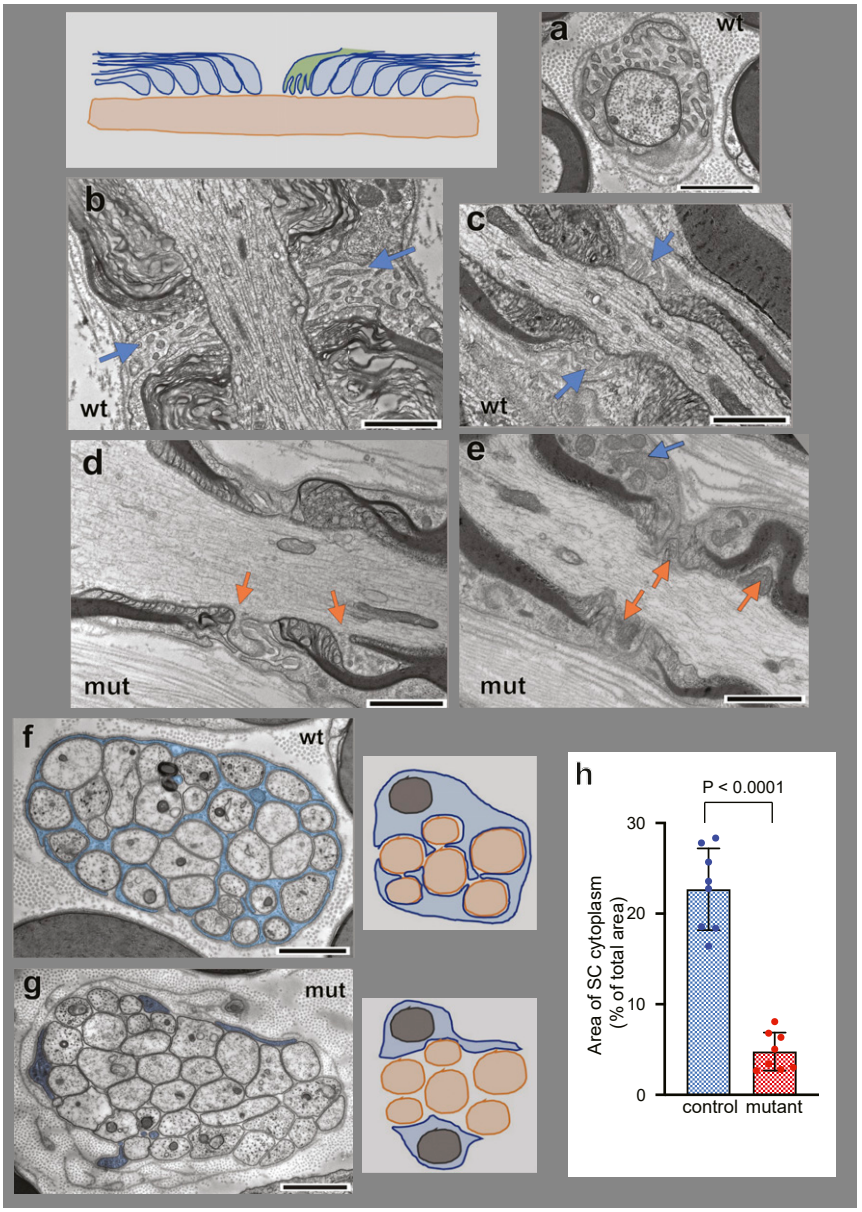

Fig. 5. EM analysis of nodes of Ranvier and nonmyelinating SCs in sciatic nerves of 12-wk-old control and PI4KB mutant mice. A simplified schematic shows the positions of the paranodal loops (blue) and the microvilli (green). (*A*) Microvilli in a cross-section of the node of Ranvier in control sciatic nerves. No such structures are recognizable in mutant nerves. (*B* and *C*) Note the prominent microvilli (blue arrows) in nodes of Ranvier in longitudinal sections in the control nerves. (*D* and *E*) Microvilli are almost completely missing in mutant nerves where often herniations of the axons can be observed (orange arrows). In many cases, SC extensions into the nodes of Ranvier are rich in mitochondria (blue arrow in *E*). (*F*) The cytoplasm of nonmyelinating SCs completely isolate the small diameter fibers in the Remak bundles in control nerves (colored blue) whereas they are unable to do so in the mutant (*G*). The simplified schematic is added to explain this defect. (*H*) Quantification of the SC cytoplasm as a percent of total Remak bundle area. (Mean ± SD is shown from analysis of 14 Remak bundles from both control and mutant animals.) Images were obtained in two independent nerve preparations from different pairs of mice, and the changes shown are the best representations of at least 10 images obtained in each experiment. (Scale bars: 1 μm.)

This was associated with separated basal lamina that surrounded these Remak bundles. Similar defects are characteristic of impaired or delayed SC differentiation (39, 40). However, the persistence of this aberration at 2 mo of age and the normal myelination of small diameter axons suggest that this defect of the Remak bundles is unlikely to reflect an SC differentiation delay. Many of these defects could be attributed to a defective cell adhesion. This would explain the inability of SCs to penetrate and wrap the Remak bundles, or the greatly reduced areas of appositions of the abaxonal membrane with the myelin surrounding the Cajal bands. The structural aberrations at the nodes of Ranvier reflected in the altered microvilli and neurofascin distribution can also be caused by impaired adhesion.

To explain the connection between PI4KB, impaired PI4P formation at the Golgi, and the structural changes, we determined the localizations of PI4KB and selected PI4P effectors in sciatic nerves of control and mutant mice. In control nerves, both PI4KB and two of its PI4P effectors, OSBP and GOLPH3, showed the expected localization to the perinuclear Golgi. Surprisingly, we also found that PI4KB prominently localized to the nodes of Ranvier in the SC microvilli, without any Golgi markers or any of the two PI4P effectors. In mutant nerves, PI4KB was undetectable and so was GOLPH3 while OSBP showed greatly reduced punctate localization that did not show tight colocalization with the residual Golgi compartment. The prominent impairment of microvilli in the nodes of Ranvier of mutant nerves suggested that PI4KB in this location is critical for the formation and function of this structure. We suspected that Rab11, a small GTP binding protein, which associates with PI4KB (21, 22, 41), might function along with PI4KB in the microvilli. However, we found no colocalization of the two proteins in this area, Rab11 being mostly present in the paranodes. Therefore, the mechanism and the effector proteins that mediate the actions of PI4KB in the microvilli remain to be elucidated.

The complete loss of GOLPH3 in SCs of mutant nerves suggested that this protein is recruited to the Golgi primarily by PI4KB in these cells. GOLPH3, which has been initially identified as an oncoprotein (42, 43), has been linked to Golgi positioning (23), as well as to directional trafficking and cell migration (6). Lack of GOLPH3 localization in a phosphatidylinositol (PI)

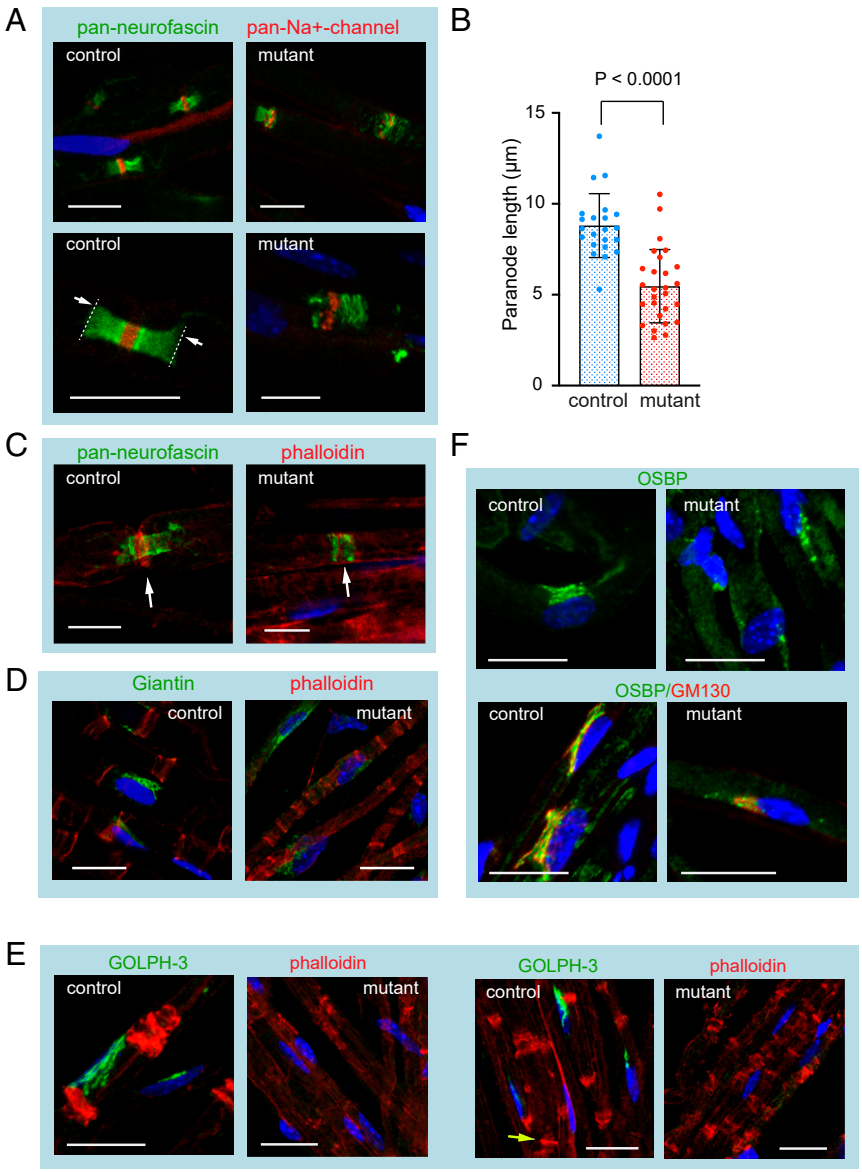

Fig. 6. Aberrant nodes of Ranvier and loss of Golgi localization of the PI4P effectors GOLPH3 and OSBP in sciatic nerves of control and PI4KB mutant mice. (*A*) Teased sciatic nerves from 13-wk-old control and mutant mice were immunostained with antibodies against all isoforms of neurofascin (green) and voltage-gated Na^+ channels (red). Note the very tight localization of neurofascin in the paranode at Ranvier in control nerves and its irregular staining in the mutants. (*B*) Quantification of paranodal length based on neurofascin staining as shown by the dotted lines and arrows in panel *A*. (Mean ± SD is shown from 22 control and 27 mutant nodes analyzed from three different nerve preparations each.) (*C*) Notable is the loss of actin enrichment in the microvilli of the nodes in the mutant nerves as shown by the white arrows (11 wk). (Scale bars: *A* and *C*, 10 μm.) (*D*) Teased sciatic nerves from 11-wk-old control and mutant mice were immunostained with phalloidin (red) and an antibody against giantin (green). Note the disorganization of the Golgi complex in the mutant nerves. (*E*) Nerves (13 to 18 wk) were stained for GOLPH3 and phalloidin. Note the Golgi localization of GOLPH3 but not in the nodes of Ranvier (yellow arrow) in control nerves. No GOLPH3 signal is detected in the mutants. (*F*) Also notable is the tight Golgi localization of OSBP in the controls and a reduced punctate signal in the mutant that no more localizes to the remaining Golgi (GM130) (analyzed at 9- to 13-wk-old mice). Pictures are maximum intensity projections from z-sections. These images are representatives of what was observed in at least two separate nerve preparations from different animals immunostained independently (Scale bars: *D*–*F*, 20 μm.)

transfer protein-deficient mice model caused migration defects of cortical neurons (44). However, GOLPH3 and its yeast homolog, Vps74, has also been shown to determine the localization of some of the glycosylating enzymes in the Golgi (25, 26). Therefore, we looked at signs of glycosylation defects in the sciatic nerves of PI4KB mice using fluorescent lectins, which are known to decorate glycoproteins and glycolipids. These experiments showed high enrichment of several lectins in the nodes of Ranvier and a significant loss of staining with a few selected lectins in this compartment. Similarly, a Western analysis showed altered lectin staining patterns of several proteins in nerves isolated from mutant animals. These results suggested that altered glycosylation of proteins could contribute to the pathologies observed in the PI4KB mutant mice. Since most cell adhesion molecules are glycosylated (45), it is likely that the suspected adhesion defect is related to the missorting or glycosylation defect of one or more of the cell adhesion molecules.

Selected molecules important for the proper adhesion of various aspects of SC anatomy were tested. For example, neurofascins were still localized to the nodes of Ranvier even if their distribution was grossly altered. Similarly, Drp2, the molecule responsible for the adhesions between the Cajal bands (46), still showed localization to the greatly reduced and smaller adhesions, but its level was severely reduced. Indeed, it has been shown that Drp2 KO nerves display disrupted appositions and Cajal bands and the mice have local hypermyelination (46). Interestingly, the Drp2 KO mice also showed very subtle functional defects and no loss of conduction velocity (46). A slightly enhanced myelination in small diameter axons was also observed in this study although large axons were clearly hypomyelinated. It is not clear whether these alterations in Drp2 reflected a defective function of the proteins or were merely the consequences of the structural defects caused by other factors. The more pleiotropic defects seen in this study, however, suggest a more complex adhesion defect beyond Drp2 function.

A recent study showed that GlcNAc-6-O-sulfation of the P_0 (MPZ) protein was critical for the adhesion of paranodal loops to the axons at the nodes of Ranvier and mice lacking the GlcNAc6ST-1 enzyme developed myelination defects (47). P_0 has been shown to be Golgi localized in SC bodies (48). In the present study, the amount of P_0 protein was greatly reduced, but it did not show altered migration in the SDS gels, which would

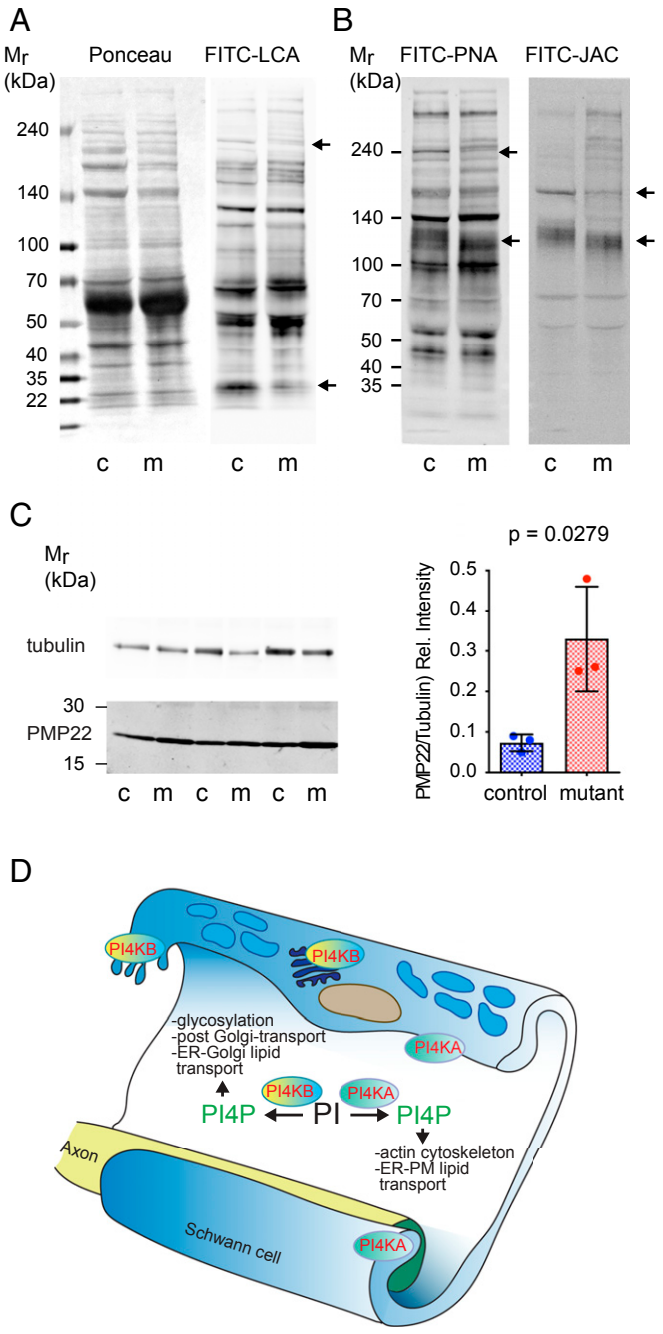

Fig. 7. Western blot analysis of proteins obtained from sciatic nerves of control and mutant mice using selected lectins and simplified scheme of the roles of PI4KA and PI4KB in SC myelination. (*A* and *B*) Proteins extracted from sciatic nerves of 12-wk-old mice were separated by SDS/PAGE and transferred to nitrocellulose membranes. The membranes were incubated with the indicated fluorescent lectins and analyzed in a fluorescence image analyzer. The arrows point molecular mass regions where most differences can be observed between the control (c) and mutant (m) nerves. (*C*) Western blot analysis of the myelin protein PMP22 in sciatic nerves from control (c) and mutant (m) mice. The level of this protein was significantly higher in mutant nerves (mean ± SD is shown). (*D*) A schematic showing the suggested roles of two PI4K enzymes in SC function. PI4KA, an enzyme primarily responsible for plasma membrane PI4P formation, controls phosphatidylserine synthesis and transport at ER-PM and is involved in proper actin dynamics (20). PI4KB, in contrast, is primarily Golgi localized and controls nonvesicular cholesterol and ceramide transport between the ER and the Golgi, and post-Golgi vesicular trafficking. Through these actions, it also regulates protein glycosylation.

indicate a glycosylation defect. Since genetic inactivation of P_0 in mice causes severe myelination defects and prominent motor defects but no major aberration in nonmyelinating SCs (49), it is unlikely that the defects observed in this study can be attributed solely to the reduced level of this protein. Nevertheless, it is quite probable that it contributed to the hypomyelination of the large diameter axons. Another important protein for myelination, PMP22, is also N-glycosylated. PMP22 duplication leads to CMT type 1A (50). Curiously, heterozygous PMP22 deletion causes hereditary neuropathy with liability to pressure palsies (51), and point mutations of the protein cause CMT type 1E (31). In the present study, the level of PMP22 was increased, rather than decreased, again with no detectable difference in its migration in SDS gels, but the relevance of these changes to the observed pathology remains to be determined.

Since OSBP is critical for the transport of cholesterol out of the ER to the Golgi, it was of interest to determine the cholesterol content of sciatic nerves of control and mutant mice. This analysis showed a greatly reduced cholesterol content of the mutant nerves (by ~70% decrease) compared to controls, even if the total lipid content of the nerves was also reduced by about 60% (Table 1). Lipidomic analysis of the nerves also showed a major decrease in the amounts of SM and PE that was disproportionally larger than the loss in the total lipid amount (note that mol% of SM and PE of total lipids is shown in Table 1). While the total cholesterol decrease could reflect the loss of the total lipid mass, the cellular distribution of cholesterol could also have been affected as expected when OSBP function is impaired. The SM changes were then consistent with the impaired functions of the ceramide transfer protein, CERT (52). Both OSBP and CERT require Golgi PI4P made by PI4KB (53, 54) for proper transport of the lipid from the ER to the Golgi, and, in the case of ceramide, its transport is critical for sphingomyelin synthesis. These lipid changes could explain the striking reduction of caveolae detected on the surface of SCs in sciatic nerves of mutant mice. Cholesterol depletion in the PM could also affect the proper localization and function of some of the PM proteins that are important for proper myelination. These data also suggested that SCs largely rely on their own cholesterol-synthesizing machinery, as already suggested by earlier studies (55, 56), and cholesterol biosynthesis was found critical for myelination through supporting mammalian target of rapamycin (mTOR) and Akt signaling in SCs (57). Likewise, cholesterol levels were found to be critical for myelination in the central nervous system (58, 59). The selective loss of PE in the mutant nerves, however, still awaits proper explanation.

Finally, it is intriguing to compare the myelination defects caused by the SC-specific inactivation of PI4KA (20) and PI4KB described in the present study (Fig. 7*D*). PI4KA mutant mice showed very profound progressive myelination defects that led to severe motor deficiencies. The lipid profile of the nerves of PI4KA mice implicated PS and PE as the primary lipids affected and a more severe loss of total lipids from the nerves. The myelination defect in PI4KA mice affected axons of all diameters yet did not cause the same defects in the nonmyelinating SCs or Remak bundles. The more subtle phenotype with very characteristic structural changes in the PI4KB mutant is consistent with the important but nonessential nature of the PI4KB enzyme at the cellular level.

In summary, the current studies have shown that PI4KB is an important component of the myelination process in peripheral nerves, supporting several aspects of Golgi function, including sterol and sphingolipid transport, glycosylation, and most likely the trafficking of proteins that are important for the process. The unexpected presence of the enzyme in the microvilli of SCs at the nodes of Ranvier, together with the defective microvilli in the nodes of mutant mice, revealed an important function of PI4KB within the PNS, which requires further studies to explore.

Table 1. Lipid changes in sciatic nerves of mice with SC-specific deletion of PI4KB

	Control	Mutant
Total lipids, nmol/μg wet weight		
8 wk	212.7	64.9
13 wk	164.7	78.7
Cholesterol, μg/mg wet weight	31.3 ± 2.9 (SD, $n = 4$)	9.6 ± 3.3 (SD, $n = 4$)
Sphingomyelin, mol% of total lipids	10.1 ± 0.8 (range, $n = 2$)	3.3 ± 0.6 (range, $n = 2$)
Phosphatidylethanolamine, mol% of total lipids	5.1 ± 0.1 (range, $n = 2$)	2.8 ± 0.3 (range, $n = 2$)

Materials and Methods

Antibodies and Chemicals. Antibodies and chemicals used in this paper are listed in *SI Appendix*, Tables S1 and S2.

Generation of Mice. All experiments with animals described in this study were approved by and conducted in full accordance with the American Association for the Accreditation of Laboratory Animal Care and the Institutional Animal Care and Use Committee (IACUC) of the National Institute of Child Health and Human Development (NICHD). Animals were housed in the NIH Bldg 35 mouse facility on ventilated racks using Tecniplast (four mice per cage) or Allentown (five mice per cage) mouse cages with air pressure negative to the room. Mice were kept on Rodent NIH NIH-07 Zeigler 241-0710-75-53 diet formulated for reproduction and lactation and were supplemented with fruits per instruction from a veterinarian. All cages use Beta Chip Bedding and Nestlets and Plastic Tubes (mouse-tunnel) for environmental enrichment.

A 9.39 kilobase (kb) region used to construct the targeting vector was first subcloned from a positively identified C57BL/6 bacterial artificial chromosome (BAC) clone (RP23: 31H18) using a homologous recombination-based technique. The region was designed such that the short homology arm (SA) extends 1.95 kb 3′ to the LoxP/FRT-flanked Neo cassette. The long homology arm (LA) extends 5.88 kb 5′ to the single LoxP site. The single LoxP site is inserted 268 base pairs (bp) upstream of exon 6, and the LoxP/FRT-flanked Neo cassette is inserted downstream of exon 7. The size of the target region is 1.56 kb containing exons 6 and 7. The targeting vector was confirmed by restriction analysis after each modification step, and by sequencing using primers designed to read from the selection cassette into the 3′ end of the target region (N2) and the 5′ end of the SA (N1). The single LoxP site was confirmed by sequencing with primer LOX1. Primers P6 and T73 anneal to the vector sequence and read into the 3′ and 5′ ends of the BAC sub clone. Additional primers P1 and P4 were used to confirm that no errors were incorporated in the modified region (*SI Appendix*, Fig. S1). The linearized targeting vector was transfected into BA1 (C57BL/6 × 129/SvEv) embryonic stem cells (Ingenious Targeting Laboratory, Ronkonkoma, NY). Correctly targeted embryonic stem cells were identified by PCR and Southern blotting. The neomycin cassette was removed by crossing F1 mice to mice expressing FLP recombinase. Mice were then backcrossed to C57BL/6 mice at GlaxoSmithKline to derive the Pi4kb conditional KO mouse colonies, which were then cross-bred with B6N.FVB-Tg(Mpz-cre)26Mes/J transgenic mice (19), from The Jackson Laboratory, in order to selectively inactivate PI4KB only from SCs.

Immunohistochemistry with the Teased Sciatic Nerve Fibers. Both sides of sciatic nerves were removed from control (control were: fl/wt Cre^+, fl/fl Cre^-, or fl/wt Cre^- littermates) or mutant mice and fixed with 4% paraformaldehyde (PFA) in phosphate-buffered saline (PBS) for 30 min at room temperature without perfusion. After washing with PBS, the nerves were teased with forceps on a coated slide glass and dried overnight at room temperature. We avoided freezing the samples for storage when staining for Golgi as freezing disrupted the structure of the Golgi in our hand. For immunocytochemistry, the slides were permeabilized with acetone at −20° for 10 min and washed with PBS for 5 min two times. Samples were then incubated with blocking buffer (2% bovine serum albumin [BSA] with 0.5% Triton X-100 in PBS) for 1 h. When mouse antibodies were used, the samples were incubated with 0.1 mg/mL Fab fragment of Goat anti-mouse immunoglobulin G (IgG) in PBS at room temperature for 1 h, to block endogenous IgG in the nerves, and washed with PBS twice for 5 min. The primary antibody was diluted with the blocking buffer and incubated with the prepared samples overnight at 4 °C. After washing with PBS for 5, 10, and 5 min, secondary antibodies diluted with the blocking buffer were applied to the samples for 1 h. After washing with PBS three times, samples were mounted by a mounting solution (Fluoromount G) containing DAPI. Images were taken with an LSM710 Zeiss scanning confocal microscope (Zeiss).

Lectin Staining. For the fixed nerves, the teased sciatic nerves were prepared and permeabilized as described in *Immunohistochemistry with the Teased Sciatic Nerve Fibers*. After washing with PBS twice for 5 min, the nerves were incubated with 20 μg/mL fluorescently labeled lectin in PBS for 1 h at room temperature. Nerves were then washed with PBS three times and mounted with the mounting solution. For Western blotting, sciatic nerves were lysed with T-PER Tissue Protein Extraction Reagent (Thermo Fisher Scientific). Protein concentrations of the lysates were measured by the bicinchoninic acid assay (BCA) assay. Samples, equivalent of 20 μg of whole proteins, were run by sodium dodecyl sulfate polyacrylamide gel electrophoresis (SDS/PAGE) and transferred onto nitrocellulose membranes. Membranes were blocked with 1% BSA in PBS overnight at 4 °C. Then, 20 μg/mL FITC-labeled lectin in 1% BSA in PBS was reacted with the membrane for 1 h at room temperature and washed with PBS for 10 min three times. FITC was detected with the ChemiDoc MP imaging system (Bio-Rad).

G-Ratio Measurement. G-ratio is a value of axonal diameter divided with myelin diameter. EM images were imported into Fiji, and Feret's diameter of myelin measured by Fiji was used for calculation of g-ratio.

Rotarod Test. Mice were placed in a testing room for at least 1 h for their acclimation. Then, the mice were put on a rotating rod at 5 rpm in separate lanes for 60 s. This procedure was repeated three times, separated by an internal interval of 10 min. After that, the mice were placed on the rod rotating at speed accelerating from 5 to 40 rpm in 300 s, and the time when the mice fell from the rod was recorded. This test was done five times with intervals of 15 min. A value of one experiment was the average of the records from the five trials.

Nerve Conduction Velocity Measurement. Mice (P60) were anesthetized with 2% isoflurane in 100% oxygen, and the fur covering the hind limbs was shaved and depilated with a commercially available hair-removal cream. The sensing electrode was placed at the position where the gastrocnemius muscle has its maximum diameter while the reference electrode was placed just distal to it. To target the sciatic nerve accurately, a small incision was made, and distal and proximal stimulation of the nerve was performed using a monopolar disposable 30 G needle electrode (cat. no. S53153; Natus). Stimuli were delivered by a Grass model S48G stimulator and were monitored with a Coulbourn Instruments model V75-04 amplifier with 100× gain and bandpass filtered between 150 Hz and 1 kHz. Stimulus and response voltage data were digitized using a National Instruments USB-6212 acquisition card and Labview Software. Analysis was carried out using custom software implemented in Matlab. Conduction time was determined as the interval from stimulus onset to the time where the tangent to the initial deflection of the muscle recording intersected the abscissa. Measurements were taken at points both distal and proximal to the spinal cord, and the conduction velocity was determined as the distance between the two recording sites divided by the difference in conduction times.

Sample Preparation for Lipidomic Analysis. Identical segments of sciatic nerves were removed from euthanized animals, and their wet weights were measured and recorded. The two nerves from one animal were then combined and homogenized in a Bullet Blender homogenizer (Next Advance Inc.,Troy, NY) using PBS, and their volume was adjusted to 1 mL. Then, 100 μL of this sample was used for cholesterol measurement, and 30 μL was used for lipidomic analysis performed by Lipotype GmbH (Dresden, Germany).

Cholesterol Analysis. Sample preparation was conducted as previously described by Kelley with slight modifications (60). Briefly, 100 μL of homogenate was diluted into 1 mL of 1× PBS. Five micrograms of coprostan-3-ol (Sigma) was added to each sample as a surrogate internal standard. The samples were saponified in 4% potassium hydroxide (KOH) in 70% ethanol for 1 h at 60 °C. Samples were then extracted with an equal volume of ethyl acetate and centrifuged for 5 min at 2,200 revolutions per minute. The organic phase was removed and dried under a stream of nitrogen. The samples were derivatized with bis-trimethylsilyltrifluoroacetamide (BSTFA) plus 1% trimethylchlorosilane (TMCS) (Thermo Fisher Scientific) for 1 h at 60 °C. Derivate samples were injected onto a gas chromatogram/mass spectrometer (Trace 1310GC TSQ 8000 Evo Mass Spectrometer; Thermo Scientific) utilizing a ZB-1701 30 m × 0.32 mm × 0.25 μm column (Phenomenex). On injection, the oven temperature was 170 °C and ramped at 21 °C per minute to 250 °C and then ramped at 3 °C per minute to a final temperature of 290 °C. Total amounts of cholesterol were determined based on comparison to the surrogate internal standard coprostan-3-ol. Retention times were confirmed using standards (Sigma) of the available compounds, and the National Institutes of Standards and Technology mass spectral library, data version 14.

EM. After anesthetizing 2-mo-old mice with 2% isoflurane in 100% oxygen, transcardial perfusion fixation was performed on a downdraft table equipped with a chemical waste collection system. Phosphate buffer was perfused briefly (<5 min) through the left ventricle, followed immediately by a fixative solution consisting of 4% paraformaldehyde and 2.5% glutaraldehyde in phosphate buffer. Excised sciatic nerve samples were postfixed for 72 h in the same fixative at 4 °C. In preparation for resin embedding, nerve samples were equilibrated in 0.1 M sodium cacodylate buffer, intensified in 2% osmium tetroxide (OsO_4), dehydrated through a graded ethanol series, and equilibrated to 100% propylene oxide. Next, an Embed-812 resin (Electron Microscopy Sciences, Hatfield, PA.) infiltration series, using propylene oxide as the solvent, up to 100% resin, was completed. The epoxy resin was polymerized for 24 h in a vacuum oven set at 60 °C. Ultrathin sections (80 nm) were prepared on a Reichert-Jung Ultracut-E ultramicrotome using a Diatome diamond knife (Electron Microscopy Sciences, Hatfield, PA). The ultrathin sections were transferred to 300 mesh cooper grids (Electron Microscopy Sciences, Hatfield, PA) and were poststained with uranyl acetate and lead citrate. Imaging was performed on a JEOL 1400 transmission electron microscope operating at 80 kV.

Statistical Analysis. Most of the analyses were carried out using the two-tailed Student's *t* test with Welch correction. When comparisons were between more than two groups, one-way ANOVA analysis was performed, followed by Tukey's multiple comparisons test. The values are expressed as mean ± SEM, and all statistical analyses were performed using GraphPad Prism, version 8.4.

Data Availability. All study data are included in the article and *SI Appendix*.

ACKNOWLEDGMENTS. This work was supported in part by the intramural research program of the Eunice Kennedy Shriver NICHD at the NIH. Confocal imaging and EM analysis were performed at the Microscopy and Imaging Core of the NICHD, with the kind assistance of Dr. Vincent Schram, Lynne Holtzclaw, and Louis (Chip) Dye. We thank Drs. Christopher Wassif and Forbes Porter (NICHD) for cholesterol analysis; and Dr. Peter Brophy (University of Edinburgh) for the Drp2 and pan-neurofascin antibodies used in this study.

1. M. L. Feltri, Y. Poitelon, S. C. Previtali, How Schwann cells sort axons: New concepts. *Neuroscientist* **22**, 252–265 (2016).
2. D. Pareyson, P. Saveri, C. Pisciotta, New developments in Charcot-Marie-Tooth neuropathy and related diseases. *Curr. Opin. Neurol.* **30**, 471–480 (2017).
3. C. Bucci, O. Bakke, C. Progida, Charcot-Marie-Tooth disease and intracellular traffic. *Prog. Neurobiol.* **99**, 191–225 (2012).
4. P. N. Devreotes *et al*., Excitable signal transduction networks in directed cell migration. *Annu. Rev. Cell Dev. Biol.* **33**, 103–125 (2017).
5. S. Yadav, S. Puri, A. D. Linstedt, A primary role for Golgi positioning in directed secretion, cell polarity, and wound healing. *Mol. Biol. Cell* **20**, 1728–1736 (2009).
6. M. Xing *et al*., GOLPH3 drives cell migration by promoting Golgi reorientation and directional trafficking to the leading edge. *Mol. Biol. Cell* **27**, 3828–3840 (2016).
7. Y. Zhang *et al*., Assembly and maintenance of nodes of ranvier rely on distinct sources of proteins and targeting mechanisms. *Neuron* **73**, 92–107 (2012).
8. T. Yamaji, K. Hanada, Sphingolipid metabolism and interorganellar transport: Localization of sphingolipid enzymes and lipid transfer proteins. *Traffic* **16**, 101–122 (2015).
9. G. D'Angelo, M. Vicinanza, C. Wilson, M. A. De Matteis, Phosphoinositides in Golgi complex function. *Subcell. Biochem.* **59**, 255–270 (2012).
10. Y. J. Wang *et al*., Phosphatidylinositol 4 phosphate regulates targeting of clathrin adaptor AP-1 complexes to the Golgi. *Cell* **114**, 299–310 (2003).
11. G. D'Angelo *et al*., Glycosphingolipid synthesis requires FAPP2 transfer of glucosylceramide. *Nature* **449**, 62–67 (2007).
12. B. Antonny, J. Bigay, B. Mesmin, The oxysterol-binding protein cycle: Burning off PI(4)P to transport cholesterol. *Annu. Rev. Biochem.* **87**, 809–837 (2018).
13. E. Boura, R. Nencka, Phosphatidylinositol 4-kinases: Function, structure, and inhibition. *Exp. Cell Res.* **337**, 136–145 (2015).
14. S. Minogue, The many roles of type II phosphatidylinositol 4-kinases in membrane trafficking: New tricks for old dogs. *Bioessays* **40**, 10.1002/bies.201700145 (2018).
15. C. Wilson *et al*., The Golgi apparatus: An organelle with multiple complex functions. *Biochem. J.* **433**, 1–9 (2011).
16. N. Altan-Bonnet, T. Balla, Phosphatidylinositol 4-kinases: Hostages harnessed to build panviral replication platforms. *Trends Biochem. Sci.* **37**, 293–302 (2012).
17. J. G. Donaldson, A. Honda, R. Weigert, Multiple activities for Arf1 at the Golgi complex. *Biochim. Biophys. Acta* **1744**, 364–373 (2005).
18. Y. Miyamoto *et al*., BIG1/Arfgef1 and Arf1 regulate the initiation of myelination by Schwann cells in mice. *Sci. Adv.* **4**, eaar4471 (2018).
19. M. L. Feltri *et al*., P0-Cre transgenic mice for inactivation of adhesion molecules in Schwann cells. *Ann. N. Y. Acad. Sci.* **883**, 116–123 (1999).
20. A. Alvarez-Prats *et al*., Schwann-cell-specific deletion of phosphatidylinositol 4-kinase alpha causes aberrant myelination. *Cell Rep.* **23**, 2881–2890 (2018).
21. G. Polevoy *et al*., Dual roles for the Drosophila PI 4-kinase four wheel drive in localizing Rab11 during cytokinesis. *J. Cell Biol.* **187**, 847–858 (2009).
22. P. de Graaf *et al*., Phosphatidylinositol 4-kinasebeta is critical for functional association of rab11 with the Golgi complex. *Mol. Biol. Cell* **15**, 2038–2047 (2004).
23. H. C. Dippold *et al*., GOLPH3 bridges phosphatidylinositol-4- phosphate and actomyosin to stretch and shape the Golgi to promote budding. *Cell* **139**, 337–351 (2009).
24. B. Mesmin *et al*., A four-step cycle driven by PI(4)P hydrolysis directs sterol/PI(4)P exchange by the ER-Golgi tether OSBP. *Cell* **155**, 830–843 (2013).
25. K. R. Schmitz *et al*., Golgi localization of glycosyltransferases requires a Vps74p oligomer. *Dev. Cell* **14**, 523–534 (2008).
26. N. A. Pereira, H. X. Pu, H. Goh, Z. Song, Golgi phosphoprotein 3 mediates the Golgi localization and function of protein O-linked mannose β-1,2-N-acetylglucosaminyltransferase 1. *J. Biol. Chem.* **289**, 14762–14770 (2014).
27. E. S. Eckert *et al*., Golgi phosphoprotein 3 triggers signal-mediated incorporation of glycosyltransferases into coatomer-coated (COPI) vesicles. *J. Biol. Chem.* **289**, 31319–31329 (2014).
28. T. Hoshi *et al*., Nodal protrusions, increased Schmidt-Lanterman incisures, and paranodal disorganization are characteristic features of sulfatide-deficient peripheral nerves. *Glia* **55**, 584–594 (2007).
29. K. A. Sheikh, T. J. Deerinck, M. H. Ellisman, J. W. Griffin, The distribution of ganglioside-like moieties in peripheral nerves. *Brain* **122**, 449–460 (1999).
30. W. J. Streit, B. A. Schulte, S. S. Spicer, J. D. Balentine, Histochemical localization of galactose-containing glycoconjugate at peripheral nodes of Ranvier in the rat. *J. Histochem. Cytochem.* **33**, 33–39 (1985).
31. J. Li, B. Parker, C. Martyn, C. Natarajan, J. Guo, The PMP22 gene and its related diseases. *Mol. Neurobiol.* **47**, 673–698 (2013).
32. H. T. Park, J. K. Kim, N. Tricaud, The conceptual introduction of the "demyelinating Schwann cell" in peripheral demyelinating neuropathies. *Glia* **67**, 571–581 (2019).
33. B. D. Trapp *et al*., Polarization of myelinating Schwann cell surface membranes: Role of microtubules and the trans-Golgi network. *J. Neurosci.* **15**, 1797–1807 (1995).
34. K. O. Schink, K. W. Tan, H. Stenmark, Phosphoinositides in control of membrane dynamics. *Annu. Rev. Cell Dev. Biol.* **32**, 143–171 (2016).
35. C. A. Flanagan *et al*., Phosphatidylinositol 4-kinase: Gene structure and requirement for yeast cell viability. *Science* **262**, 1444–1448 (1993).
36. C. Walch-Solimena, P. Novick, The yeast phosphatidylinositol-4-OH kinase pik1 regulates secretion at the Golgi. *Nat. Cell Biol.* **1**, 523–525 (1999).
37. J. A. Brill, G. R. Hime, M. Scharer-Schuksz, M. T. Fuller, A phospholipid kinase regulates actin organization and intercellular bridge formation during germline cytokinesis. *Development* **127**, 3855–3864 (2000).
38. J. Burgess *et al*., Type II phosphatidylinositol 4-kinase regulates trafficking of secretory granule proteins in Drosophila. *Development* **139**, 3040–3050 (2012).
39. J. L. Salzer, Schwann cell myelination. *Cold Spring Harb. Perspect. Biol.* **7**, a020529 (2015).
40. D. R. Zollinger, K. J. Chang, K. Baalman, S. Kim, M. N. Rasband, The polarity protein Pals1 regulates radial sorting of axons. *J. Neurosci.* **35**, 10474–10484 (2015).
41. J. E. Burke *et al*., Structures of PI4KIIIβ complexes show simultaneous recruitment of Rab11 and its effectors. *Science* **344**, 1035–1038 (2014).
42. K. L. Scott *et al*., GOLPH3 modulates mTOR signalling and rapamycin sensitivity in cancer. *Nature* **459**, 1085–1090 (2009).
43. R. S. Kuna, S. J. Field, GOLPH3: A Golgi phosphatidylinositol(4)phosphate effector that directs vesicle trafficking and drives cancer. *J. Lipid Res.* **60**, 269–275 (2019).
44. Z. Xie, S. K. Hur, L. Zhao, C. S. Abrams, V. A. Bankaitis, A Golgi lipid signaling pathway controls apical Golgi distribution and cell polarity during neurogenesis. *Dev. Cell* **44**, 725–740.e4 (2018).
45. R. H. Quarles, Myelin sheaths: Glycoproteins involved in their formation, maintenance and degeneration. *Cell. Mol. Life Sci.* **59**, 1851–1871 (2002).

46. D. L. Sherman, L. M. Wu, M. Grove, C. S. Gillespie, P. J. Brophy, Drp2 and periaxin form Cajal bands with dystroglycan but have distinct roles in Schwann cell growth. *J. Neurosci.* **32**, 9419–9428 (2012).
47. T. Yoshimura *et al*., GlcNAc6ST-1 regulates sulfation of N-glycans and myelination in the peripheral nervous system. *Sci. Rep.* **7**, 42257 (2017).
48. B. D. Trapp, Y. Itoyama, N. H. Sternberger, R. H. Quarles, H. Webster, Immunocytochemical localization of P0 protein in Golgi complex membranes and myelin of developing rat Schwann cells. *J. Cell Biol.* **90**, 1–6 (1981).
49. K. P. Giese, R. Martini, G. Lemke, P. Soriano, M. Schachner, Mouse P0 gene disruption leads to hypomyelination, abnormal expression of recognition molecules, and degeneration of myelin and axons. *Cell* **71**, 565–576 (1992).
50. J. R. Lupski *et al*., DNA duplication associated with Charcot-Marie-Tooth disease type 1A. *Cell* **66**, 219–232 (1991).
51. J. Li, K. Krajewski, R. A. Lewis, M. E. Shy, Loss-of-function phenotype of hereditary neuropathy with liability to pressure palsies. *Muscle Nerve* **29**, 205–210 (2004).
52. K. Hanada *et al*., Molecular machinery for non-vesicular trafficking of ceramide. *Nature* **426**, 803–809 (2003).
53. B. Mesmin *et al*., Sterol transfer, PI4P consumption, and control of membrane lipid order by endogenous OSBP. *EMBO J.* **36**, 3156–3174 (2017).
54. B. Tóth *et al*., Phosphatidylinositol 4-kinase IIIbeta regulates the transport of ceramide between the endoplasmic reticulum and Golgi. *J. Biol. Chem.* **281**, 36369–36377 (2006).
55. Q. Fu *et al*., Control of cholesterol biosynthesis in Schwann cells. *J. Neurochem.* **71**, 549–555 (1998).
56. G. Saher *et al*., Cholesterol regulates the endoplasmic reticulum exit of the major membrane protein P0 required for peripheral myelin compaction. *J. Neurosci.* **29**, 6094–6104 (2009).
57. E. S. Mathews, B. Appel, Cholesterol biosynthesis supports myelin gene expression and axon ensheathment through modulation of P13K/Akt/mTor signaling. *J. Neurosci.* **36**, 7628–7639 (2016).
58. G. Saher *et al*., High cholesterol level is essential for myelin membrane growth. *Nat. Neurosci.* **8**, 468–475 (2005).
59. G. Saher, S. K. Stumpf, Cholesterol in myelin biogenesis and hypomyelinating disorders. *Biochim. Biophys. Acta* **1851**, 1083–1094 (2015).
60. R. I. Kelley, Diagnosis of Smith-Lemli-Opitz syndrome by gas chromatography/mass spectrometry of 7-dehydrocholesterol in plasma, amniotic fluid and cultured skin fibroblasts. *Clin Chim Acta* **236**, 45–58 (1955).